Available online at www.sciencedirect.com

ScienceDirect

JOURNAL OF IRON AND STEEL RESEARCH, INTERNATIONAL. 2016, 23(3): 244-252

Effects of Temperature and Strain Rate on Flow Behavior and Microstructural Evolution of Super Duplex Stainless Steel under Hot Deformation

Ming MA[1], Hua DING[1], Zheng-you TANG[1], Jing-wei ZHAO[2], Zhou-hua JIANG[1], Guang-wei FAN[3]

(1. School of Material Science and Engineering, Northeastern University, Shenyang 110819, Liaoning, China;
2. School of Mechanical, Materials and Mechatronic Engineering, University of Wollongong, NSW 2522, Australia;
3. Technology Center, Shanxi Taigang Stainless Steel Co., Ltd., Taiyuan 030003, Shanxi, China)

Abstract: Hot compression tests were carried out in the temperature range of 1223—1473 K and strain rate range of 0.01—30 s^{-1} to investigate the flow behavior and microstructural evolution of super duplex stainless steel 2507 (SDSS2507). It is found that most of the flow curves exhibit a characteristic of dynamic recrystallization (DRX) and the flow stress increases with the decrease of temperature and the increase of strain rate. The apparent activation energy Q of SDSS2507 with varying true strain and strain rate is determined. As the strain increases, the value of Q declines in different ways with varying strain rate. The microstructural evolution characteristics and the strain partition between the two constituent phases are significantly affected by the Zener-Hollomon parameter (Z). At a lower ln$Z$, dynamic recovery (DRV) and continuous dynamic recrystallization (CDRX) of the ferrite dominate the softening mechanism during the compression. At this time, steady state deformation takes place at the last stage of deformation. In contrast, a higher ln$Z$ will facilitate the plastic deformation of the austenite and then activate the discontinuous dynamic recrystallization (DDRX) of the austenite, which leads to a continuous decline of the flow stress even at the last deformation stage together with CDRX of the ferrite.

Key words: duplex stainless steel; hot deformation behavior; dynamic recovery; dynamic recrystallization; strain partition

Duplex stainless steels (DSSs) have the excellent combination of mechanical properties, stress corrosion resistance and weldability, and have been considered as the alternatives to the single austenitic and ferritic stainless steels in many industrial fields[1-3]. It is well known that the excellent properties of DSSs mainly rely on a duplex microstructure comprising approximately equal proportion of austenite and ferrite phases. During the hot deformation, the flow behavior of each constituent phase is severely affected by the others[4]. Generally, surface defects of products are easily caused due to the difference in thermal expansion coefficient and flow behavior between the two constituent phases[5]. Therefore, it is vital to investigate the flow behaviors of these special materials in more detail in order to seek an effective way to control the hot deformation behavior and thus improve the quality of the products.

The deformation mechanism of austenite differs largely from ferrite during hot deformation. For a single phase ferritic stainless steel, the high stacking fault energy (SFE) can make dislocations climb or cross slip easily, leading to the occurrence of dynamic recovery (DRV), sub-grain formation and other microstructural evolution mechanisms[6-9]. Differently, austenitic steel undergoes a limited DRV due to the relatively low SFE. As a result, dynamic recrystallization (DRX) will take place because of the large driving force once a critical strain is reached[10,11]. The deformation will be non-uniform when a duplex microstructure of ferrite and austenite deforms jointly. It is found that the harder austenite and softer fer-

Foundation Item: Item Sponsored by National Key Technology Research and Development Program of China (2012BAE04B01)
Biography: Ming MA, Doctor Candidate; **E-mail**: neummslq@126.com; **Received Date**: January 14, 2015
Corresponding Author: Hua DING, Doctor, Professor; **E-mail**: hding2013@163.com

rite usually cause a strain partition when deformed at high temperature[7], which has actually increased the difficulties of research on the flow behavior of DSSs. There has been ongoing controversy on the dominant softening mechanism of DSSs during hot deformation in recent years.

Some researchers[12-14] proposed that both austenite and ferrite in DSSs might soften by their own softening mechanism as in the corresponding single phase alloys. On the contrary, the study of Zou et al.[15] showed that the softening mechanism of the ferrite in DSSs would be DRX. Liu et al.[16] confirmed that the softening mechanism of ferrite phase in a DSS was quite different from that in the single phase stainless steels, and both ferrite and austenite softened by DRX. Moreover, Fan et al.[17] pointed out that DRX of austenite was inhibited in duplex structures, and only DRV occurred in the cast DSS2205. The interaction and strain partition between austenite and ferrite phases at varying temperatures and strain rates should be considered for the research on the softening mechanism of each constituent phase in DSSs. Unfortunately, the previous reports have not addressed this aspect clearly. Thus, investigations on the characteristics of flow curves, together with relevant microstructural evolution referring to the microstructural morphology and adjacent grain misorientation angle distribution of each phase become essential and significant.

Super duplex stainless steel 2507 (SDSS2507) is a typical third-generation DSS. The dynamic response mechanism and hot deformation behavior of this steel have not been clearly understood so far. In this paper, hot uniaxial compression tests were conducted under varying deformation conditions to investigate the effects of strain rate, true strain and deformation temperature on the flow behavior of SDSS2507 and verify the relation between the flow behavior and microstructural evolution.

1 Experimental Procedure

The chemical compositions of the SDSS2507 used in the present research are shown in Table 1. The cast billets were hot forged in the temperature range of 1323—1423 K and then annealed at 1323 K for 300 s followed by water quenching.

Table 1 Chemical compositions of the experimental steel

mass%

Cr	Mo	Ni	N	Mn	C	Si	S
25.21	4.23	7.08	0.26	1.08	0.03	0.37	0.02

Cylindrical specimens of 10 mm in diameter and 15 mm in height were machined with the axis parallel to the forging direction. Hot compression tests were carried out on a Gleeble-1500 thermal-mechanical simulator. The specimens were first preheated to 1423 K, and then held for 300 s followed by cooling to the preset temperature with a cooling rate of 5 K/s. The purpose of soaking at high temperature is to enhance the homogenization in the composition and microstructure of the starting materials. Prior to compression tests, each cylindrical specimen was held for 10 s at the deformation temperature to avoid radial temperature gradient. A thermocouple was welded at the middle of the specimen to monitor the actual temperature during the test.

Compression tests were conducted in strain rate range of 0.01—30 s^{-1}, temperature range of 1223—1473 K and true strain range of 0—0.8, followed by water quenching. Deformed specimens were sectioned parallel to the deformation axis and electropolished by a solution mixed with HClO, C_2H_5OH and H_2O for optical microscope (OM) and electron back-scattered diffraction (EBSD) observations, and then electropolished by a 10 mass% NaOH solution. The characterization of microstructure was investigated quantitatively by the image processing software-Image Pro-Plus, and at least twenty microstructure images were selected randomly for the measurement of each specimen.

2 Results

2.1 True stress-strain curves

Fig. 1 shows the true stress-strain curves obtained from hot compression testing under varying deformation conditions. It is clear that the effects of temperature and strain rate on the flow stress are significant. The flow stress increases with the increase of strain rate and the decrease of temperature. Meanwhile, the flow curves within the temperature range of 1223—1423 K exhibit softening characterization after a peak stress, indicating that DRX has occurred after the peak stress. When the compression is performed at 0.01—0.1 s^{-1} with all the temperatures and 1—30 s^{-1} with 1473 K, a steady state deformation occurs during the compression. By comparison, as strain rate increases and temperature decreases, the flow stress declines continuously even at the last stage of deformation. Thus, it can be concluded that strain rate and deformation temperature are the main factors that affect the flow behavior and

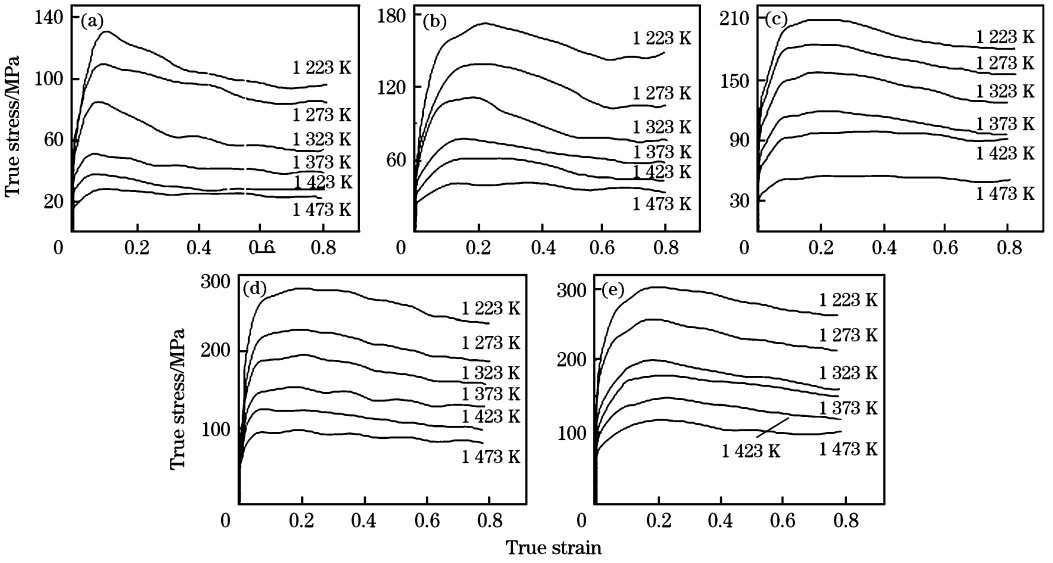

(a) $\dot{\varepsilon}=0.01\ s^{-1}$; (b) $\dot{\varepsilon}=0.1\ s^{-1}$; (c) $\dot{\varepsilon}=1\ s^{-1}$; (d) $\dot{\varepsilon}=10\ s^{-1}$; (e) $\dot{\varepsilon}=30\ s^{-1}$.

Fig. 1 True stress-true strain curves of SDSS2507 deformed under different deformation conditions

microstructural evolution of SDSS2507 during hot deformation.

2.2 Constitutive analysis

The effects of deformation temperature and strain rate on the flow behavior can be described by the Zener-Hollomon parameter, Z[18,19], as follows:

$$Z=\dot{\varepsilon}\exp\left(\frac{Q_p}{RT}\right) \tag{1}$$

where, $\dot{\varepsilon}$ is the strain rate, s^{-1}; R is the gas constant, 8.314 J·mol^{-1}·K^{-1}; T is the absolute temperature, K; and Q_p is the apparent activation energy of the hot deformation corresponding to the peak stress. Obviously, the higher the strain rate and the lower the temperature are, the larger value of Z becomes. Accordingly, the value of apparent activation energy Q corresponding to a given strain can be determined by the Arrhenius-type equation[20], as follows:

$$Q=R\left(\frac{\partial \ln\dot{\varepsilon}}{\partial \ln[\sinh(\alpha\sigma)]}\right)_T\left(\frac{\partial \ln[\sinh(\alpha\sigma)]}{\partial(1/T)}\right)_{\dot{\varepsilon}} \tag{2}$$

where α is material constant determined by the linear relation between σ, $\ln\sigma$ and $\ln\dot{\varepsilon}$, respectively. Accordingly, σ is the stress for a given strain and varies with the increase of strain in flow curves. Based on Eq. (2), the values of Q with an increasing strain can be calculated at the different strain rates, as presented in Fig. 2. For all strain rates, the Q almost decreases as the compression continues due to the softening behavior occurring in the alloy. At lower strain rates (0.01 and 0.1 s^{-1}), the value of Q decreases gradually with the increase of strain from 0.1 to 0.5 and remains almost unchanged at last stage of deformation. By comparison, when the compressions are performed at higher strain rates (10 and 30 s^{-1}), the value of Q remains the same or rises slightly within the strain range of 0.2—0.4, and then falls down once again as the deformation continues. Accordingly, the difference in the variation of Q with different strain rates is considered to be related to the different strain partitions in each phase, which will be discussed in more detail later.

2.3 Microstructural evolution

The OM images for microstructural evolution analysis have been taken in the center of axial section because it could represent the real deformation microstructure state. The light gray and dark gray areas of the microstructural images represent austenite and ferrite phases, respectively. As shown in Fig. 3(a), many coarse grains are observed in ferrite and the average size of the grains reaches 46.7 μm at the lowest ln$Z$ ($T=1473$ K, $\dot{\varepsilon}=0.01\ s^{-1}$). As the value of ln$Z$ increases, the grains of ferrite are significantly refined while the average grain size of ferrite has decreased into 3.1 μm at the highest ln$Z$ ($T=1223$ K, $\dot{\varepsilon}=30\ s^{-1}$), as shown in Fig. 3(i). Fig. 4 exhibits the average grain size of ferrite with varying values of ln$Z$. The quantitative relationship between the ferrite grain size (D_δ) and ln$Z$ can be expressed by

$$D_\delta=9.714\times10^{12}(\ln Z)^{-7.005} \tag{3}$$

For the austenite, as exhibited in Figs. 3(a)—3(d), most of the austenite islands still present almost eq-

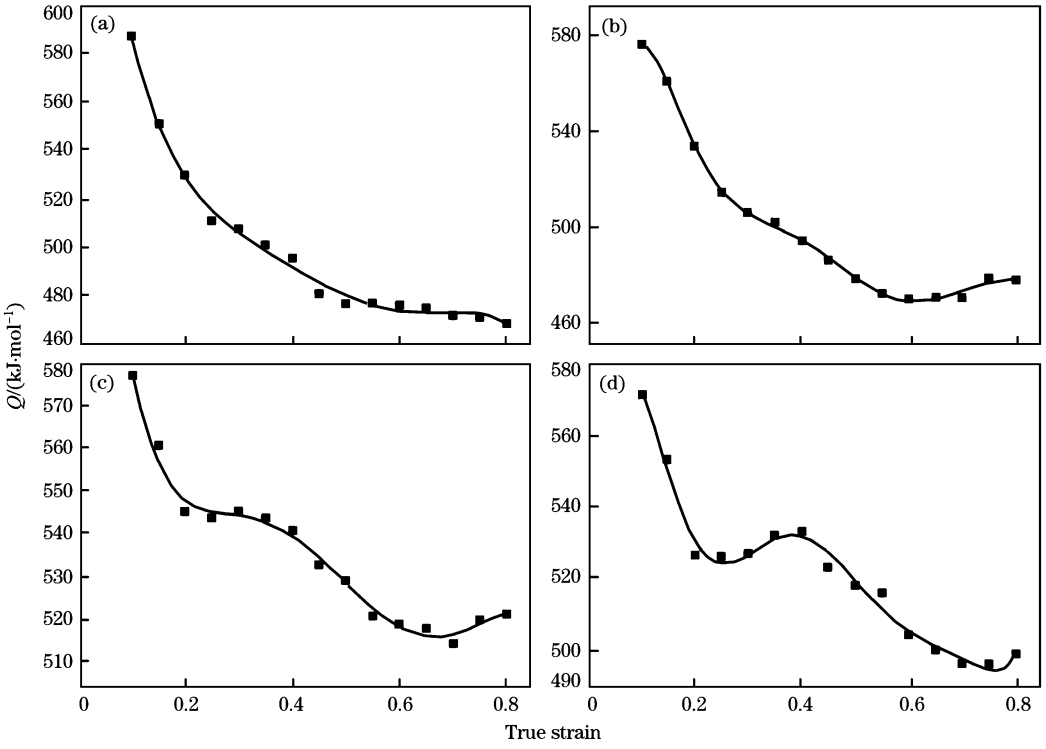

(a) $\dot{\varepsilon}=0.01\ s^{-1}$; (b) $\dot{\varepsilon}=0.1\ s^{-1}$; (c) $\dot{\varepsilon}=10\ s^{-1}$; (d) $\dot{\varepsilon}=30\ s^{-1}$.

Fig. 2 Variation in Q by increasing the strain at different strain rates

uiaxed at a lower ln$Z$, indicating that only limited deformation occurs in the austenite. Set χ as the average ratio of long to short radius of the austenite islands, and it can be found that the average χ is 5.31 when ln$Z$ is lower than 48.3. However, as seen in Figs. 3(e)—3(i), the austenite islands are obviously elongated due to the compression as the value of ln$Z$ increases, and at this time the average χ equals 12.81. However, it should be noted that the austenite islands discussed above only represent "phase units" but not "austenite grains", and the microstructural evolution of austenite grains should be further investigated. The average volume fraction of austenite phase under varying deformation temperatures is presented in Fig. 5. It can be seen that the average volume fraction of austenite phase increases as the temperature decreases because of the occurrence of $\delta\rightarrow\gamma$ phase transformation[21].

Fig. 6 shows the EBSD images at different strains, deformation temperatures and strain rates. The light and dark grey areas in the EBSD images represent austenite and ferrite phases, respectively. The white lines reveal high-angle grain boundaries (HAGBs, $\theta\geqslant15°$), and the black lines indicate low-angle grain boundaries (LAGBs, $\theta\leqslant15°$). Before compression, as presented in Fig. 6(a), the steel contains approximately half of the volume fraction of austenite phase which is embedded in the ferrite matrix. In ferrite, adjacent grain misorientation angles distribute in the range of 0—15° (Fig. 6(b)), indicating that most of grain boundaries in ferrite are LAGBs. For austenite phase, there is a certain number of HAGBs, most of which belong to the first-order twin coincidence-site lattice (CSL) characterized by 60° rotation from the [111] axis with an error of 2°. This result is consistent with the report on the flow behavior of DSS2101[16].

After straining of 0.15 at 1323 K and 0.01 s^{-1} (ln$Z$=46.0), as shown in Figs. 6(c) and 6(d), the ferrite grains are obviously refined and adjacent grain misorientation angles are still distributed in the range of 0—15°. In austenite, the morphology of islands keeps almost undeformed and the proportion of $\Sigma3$ twin boundary remains to be approximately 35%. With continuously increasing the strain to 0.8, as shown in Figs. 6(e) and 6(f), many LAGBs in ferrite are transformed into HAGBs, and the relevant proportion of HAGBs in ferrite increases significantly to 56%. In austenite, the proportion of $\Sigma3$ twin boundary declines directly to 5%. However, differing from single austenitic stainless steels, a certain number of elongated grains are observed whereas only a few

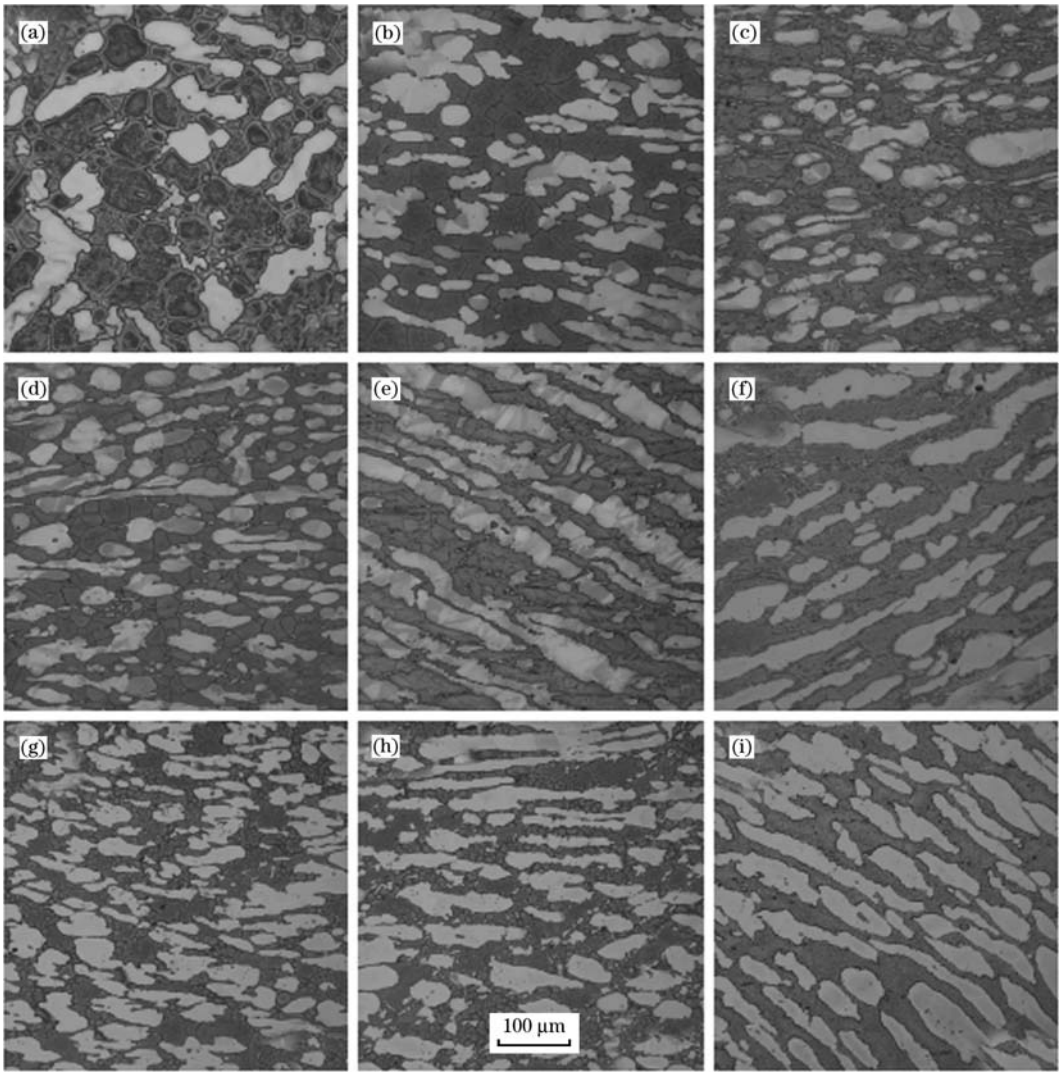

(a) $\dot{\varepsilon}=0.01\ s^{-1}$, $T=1473$ K, $\ln Z=40.8$; (b) $\dot{\varepsilon}=1\ s^{-1}$, $T=1473$ K, $\ln Z=45.5$; (c) $\dot{\varepsilon}=30\ s^{-1}$, $T=1473$ K, $\ln Z=48.3$;
(d) $\dot{\varepsilon}=0.01\ s^{-1}$, $T=1373$ K, $\ln Z=44.19$; (e) $\dot{\varepsilon}=1\ s^{-1}$, $T=1373$ K, $\ln Z=48.8$; (f) $\dot{\varepsilon}=30\ s^{-1}$, $T=1373$ K, $\ln Z=52.2$;
(g) $\dot{\varepsilon}=0.01\ s^{-1}$, $T=1273$ K, $\ln Z=50.2$; (h) $\dot{\varepsilon}=1\ s^{-1}$, $T=1273$ K, $\ln Z=54.8$; (i) $\dot{\varepsilon}=30\ s^{-1}$, $T=1273$ K, $\ln Z=58.2$.

Fig. 3 Microstructure of the specimens after deformation

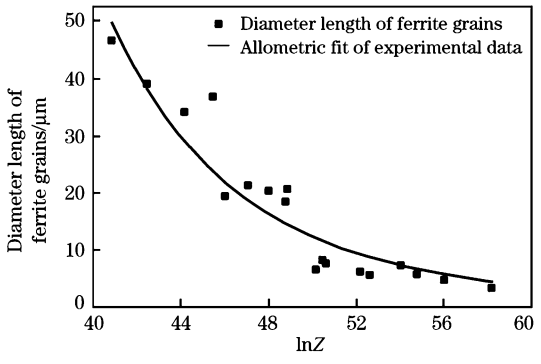

Fig. 4 Relationship between diameter length of ferrite grains and ln$Z$

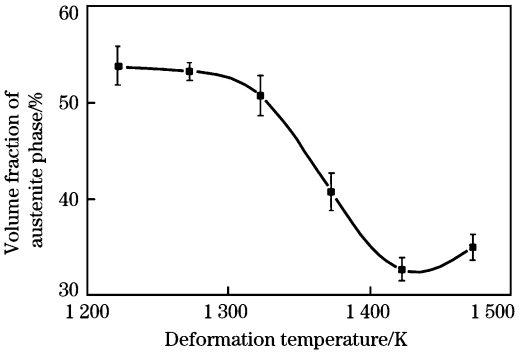

Fig. 5 Variation of volume fraction of austenite phases with deformation temperature

recrystallized grains can be found in austenite, which indicates that almost no DRX occurs under this deformation condition. Similar phenomenon can also be observed in Figs. 6(g) and 6(h) as the value of ln$Z$

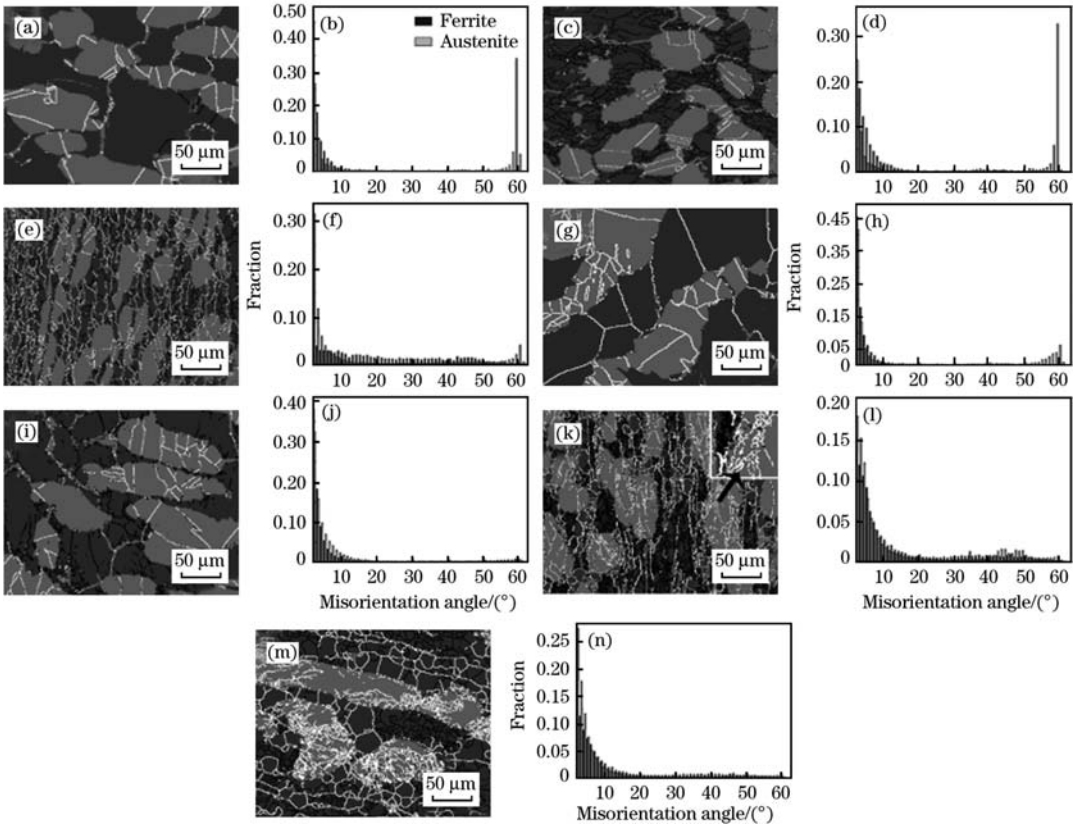

(a),(b) Before compression; (c),(d) $\dot{\varepsilon}=0.01\ s^{-1}$, $T=1323$ K, $\ln Z=46.0$, $\varepsilon=0.15$; (e),(f) $\dot{\varepsilon}=0.01\ s^{-1}$, $T=1323$ K, $\ln Z=46.0$, $\varepsilon=0.8$; (g),(h) $\dot{\varepsilon}=0.01\ s^{-1}$, $T=1473$ K, $\ln Z=40.9$, $\varepsilon=0.8$; (i),(j) $\dot{\varepsilon}=10\ s^{-1}$, $T=1323$ K, $\ln Z=52.9$, $\varepsilon=0.15$; (k),(l) $\dot{\varepsilon}=10\ s^{-1}$, $T=1323$ K, $\ln Z=52.9$, $\varepsilon=0.8$; (m),(n) $\dot{\varepsilon}=0.1\ s^{-1}$, $T=1223$ K, $\ln Z=54.8$, $\varepsilon=0.8$.

Fig. 6 EBSD image and relative adjacent grain misorientation angle distribution diagram of ferrite and austenite phases before and after deformation

decreases.

As $\ln Z$ increases to 52.9 (1323 K, 10 s^{-1}), as seen in Figs. 6(i) and 6(j), the refinement of ferrite grains is very limited after straining of 0.15 due to the fewer LAGBs formed relative to the lower $\ln Z$ shown in Fig. 6(c). As the strain increases to 0.8, as seen in Fig. 6(k), a certain number of HAGBs in ferrite have formed but there still contains 69% of LAGBs, manifesting that the transformation from LAGBs to HAGBs in ferrite is delayed at a higher $\ln Z$. In the austenite, most of annealing twins have disappeared even though only straining of 0.15 due to the plastic deformation, and the corresponding proportion of $\Sigma 3$ twin boundary has decreased to 6%. And when the strain increases to 0.8, differing from the lower $\ln Z$, a great amount of fine equiaxed grains observed in austenite islands have formed a necklace structure, indicating that the nucleation for the new grain has completed during the compression in these austenite regions. Moreover, with further increasing the value of $\ln Z$ to 54.8, similar DRX grains of austenite can be found in more austenite regions, as shown in Fig. 6(m).

3 Discussion

3.1 Flow behavior of each constituent phase

Figs. 4 and 6 indicate that the ferrite grains have been refined after compression and this phenomenon is enhanced with the increase of $\ln Z$. Generally, the dynamic softening and refinement mechanism of an alloy during hot deformation includes DRV, discontinuous DRX (DDRX) and continuous DRX (CDRX)[12-16,22]. The DDRX has a grain nucleation phenomenon of "grain boundary protruding" which usually occurs in the γ-Fe[11,16]. In the present work, DRV of ferrite firstly occurs at the beginning of deformation, as seen in Figs. 6(c) and 6(d). During this process, a lot of dislocations in the ferrite are annihilated by climb or cross slip, and others are rearranged into the LAGBs. As the deformation continues, DRX grains form with the transformation from LAGBs to HAGBs. According to this mechanism, many of the

mobile dislocations caused by plastic deformation are continuously absorbed by LAGBs, which makes LAGBs gradually rotate and then increases the relative adjacent grain misorientation angle in ferrite[23]. The phenomenon discussed above is commonly named as continuous dynamic recrystallization in previous report[24].

The softening mechanism of austenite is different from that of ferrite phase. DDRX dominates the flow behavior of austenite. DDRX is commonly characterized by nucleation and subsequent growth of new grains at high-energy sites, predominantly along grain boundaries. As presented in Fig. 6(k), a necklace structure at the grain boundaries can be observed. Accordingly, whether the DRX occurs as a continuous or a discontinuous process is mainly determined by the level of SFE of the investigated material. In high stacking fault materials, such as aluminum or α-Fe, CDRX would take place after the intense DRV. In contrast, in those low stacking fault materials such as copper or γ-Fe, DRV is significantly inhibited, causing the occurrence of DDRX as the strain increases[25].

On the other hand, as presented in Figs. 6(a) and 6(b), a large number of annealing twins form in austenite before compression. During compression, the microstructural characteristics and quantity of annealing twin boundaries have changed greatly. It can be considered that the great change of these twin boundaries is related to their interaction with the mobile dislocations. According to the reports[26,27], only a part of the mobile dislocations can pass through the twin boundaries, and the others which cannot pass through will interact with the twin boundaries, causing disappearance of the $\Sigma 3$ twin boundary.

Based on the above analysis, it can be concluded that only partial DDRX occurs within the austenite during hot compression. Ferrite undergoes a well-developed CDRX, which is slightly different from the previous study on the flow behavior of EDSS2101. The dominant softening mechanism of both austenite and ferrite are CDRX in EDSS2101[16]. The difference of flow behavior in austenite may be related to the different chemical compositions between EDSS2101 and the steel investigated in this work.

3.2 Softening mechanism of SDSS2507

Mirzaei et al.[28] proposed that the parameter Z can be used to predict the flow behavior of single austenitic stainless steels at a certain deformation temperature and strain rate. Souza et al.[29] suggested that the lower strain rate and higher temperature, the higher the migration of dislocations and grain boundaries became, which was beneficial to the occurrence of DRX during deformation of the austenitic stainless steel. But in the present work, DRX of austenite is activated with the increase of $\ln Z$ (higher strain rate and lower temperature) whereas DRX of austenite is suppressed with the decrease of $\ln Z$ although a lower Z benefits the migration of grain boundaries.

When the compression is performed in a duplex structure region, the harder austenite and softer ferrite result in a strain partition, and DRV of ferrite proceeds at the early stage of deformation as in this stage the strain energy is the driving force for softening to occur[30]. The lower strain rate and higher temperature will contribute to the dislocation climb or cross slip, and then will lead to DRV and the subsequent CDRX in ferrite being highly activated, which will successfully relief the stress concentration at ferrite grain boundaries. At this time, the flow stress in the alloy can be maintained at a relatively low level, and only a few of austenite islands yield and others are still equiaxed after compression at a lower $\ln Z$. Thus, the proportion of twin boundaries in austenite also remains unchanged at the early stage of deformation. Due to lacks of sufficient strain partition and deformation energy, as seen in Figs. 6(e) and 6(g), only very limited recrystallized structure can be observed in the austenite. Therefore, the decrease in flow stress (Fig. 1) after a peak value should be mainly related to the flow behavior of ferrite rather than austenite.

As strain rate increases and temperature decreases ($\ln Z$ increases), the annihilation and rearrangement of dislocations in ferrite are postponed at the early deformation stage due to the insufficient response time, which causes a drastically decreased number of LAGBs, as seen in Figs. 6(i) and 6(j). Undoubtedly, it will greatly increase the deformation resistance of the alloy with the increase of strain. Thus, the strain has been gradually transmitted into the harder austenite phase as the deformation continues. As a result, most of the twin boundaries only disappear after straining of 0.15, as seen in Fig. 6(j). With the increase of strain, austenite islands are seriously elongated, presenting a significant enhancement in the value of χ. And similar to single austenitic stainless steels, DDRX takes place when a critical strain for the nucleation of new

grains is reached.

In previous studies, there are many controversies on the softening mechanism of each constituent phase in DSSs. Chen et al.[12-14] found that ferrite in DSSs was softened by DRV. But Zou et al.[15,16] proposed that the dominant softening mechanism of ferrite in DSSs would be DRX. In this paper, both DRV and DRX occur in ferrite, and the degree of DRX in ferrite is mainly affected by the strain partition between ferrite and austenite phases under different deformation conditions. For austenite, DRX is inhibited due to the presence of softer ferrite, which is similar to the most circumstances in this paper. However, many DRX grains are observed in austenite when the ln$Z$ increases to a very high point. Therefore, in SDSS2507, activation of DRX of austenite phase in a duplex structure under varying deformation conditions is mainly determined by the strain partition between each constituent phase. At a lower ln$Z$, most of the strain is accommodated by the ferrite, and as a result, most of the austenite islands still present undeformed. Under this condition, DRX of austenite does not occur due to the insufficient strain. When the value of ln$Z$ increases, the plastic deformation characteristic of austenite is enhanced, presenting a relatively high value of χ after straining of 0.8. As a result, DDRX has occurred in austenite by the large driving force for the nucleation of DRX grains.

3.3 Apparent activation energy

As exhibited in Fig. 2, the curves of Q have undergone different changes with the varying strain rate. Similarly, it can also be interpreted by considering the different strain partitioning in the two constituent phases of ferrite and austenite when the strain rate changes. As proposed by many researchers, strain partitioning can be found due to the different flow responses and hardness levels between two constituent phases during hot deformation[2-4]. At a lower strain rate, DRV of the ferrite has been highly activated even at the beginning stage of deformation, leading to a large number of LAGBs after straining of 0.15, as presented in Figs. 6(c) and 6(d). In the following deformation, CDRX caused by the interaction between dislocation and LAGBs significantly reduces the dislocation density in ferrite. The flow behavior characteristic of the alloy is mainly dominated by the softer ferrite because the relatively low level of flow stress inhibits the stress transfer into the harder austenite. In the medium stage of deformation, the well-developed CDRX of ferrite relieves the stress concentration of the alloy, presenting a continuous decline in the value of Q. By comparison, at a higher strain rate, the flow stress of the alloy increases very rapidly due to the weakened DRV of ferrite which is caused by the insufficient response time, as shown in Figs. 6(i) and 6(j). When the strain increases, the enhanced deformation resistance of the alloy accelerates the stress transfer and induces the plastic deformation in many austenite islands, inducing a large number of elongated austenite islands. The austenite undergoes a very limited DRV during hot deformation due to the relatively low SFE. At the beginning of deformation, there are still no DRX occurring in austenite islands because of the insufficient strain, as presented in Fig. 6(i), which indicates a strain hardening stage in harder austenite at this time. This stage will increase the strain energy and make the further deformation of the alloy more difficult due to lacks of dynamic softening in harder austenite. Thus, the occurrence of the platform in the curve of Q at a higher strain rate is the result of interaction between the weakened dynamic softening in ferrite and increased strain hardening in austenite. However, at the last stage of deformation, CDRX of ferrite occurs although the migration of dislocation has been postponed at the early stage of deformation, as shown in Figs. 6(k) and 6(l). In addition, because of the large strain occurring in the alloy, DDRX takes place in the austenite at the last stage of deformation. Such coexistence of CDRX in ferrite and DDRX in austenite induces the second decline in the curve of Q after the platform.

4 Conclusions

(1) The flow stress of SDSS2507 increases with increasing the strain rate and decreasing the temperature. Most of the flow curves exhibit a DRX characteristic. When the compression is performed in the range of 0.01—0.1 s^{-1} at all the temperatures and 1—30 s^{-1} at 1473 K, steady state deformation occurs during the compression. By comparison, as the strain rate increases and temperature decreases, the flow stress decline continuously even at the last stage of deformation.

(2) The apparent activation energy of SDSS2507 with varying true strain and strain rate is determined. At the lower strain rates (0.01 and 0.1 s^{-1}), the value of Q decreases gradually with the increase of the strain range of 0.1 to 0.5 and then remains un-

changed. By comparison, at higher strain rates (10 and 30 s^{-1}), the decline of the value of Q is interrupted within the strain range of 0.2 — 0.4, and then falls down once again as the deformation continues. The difference in the variation of Q with varying strain rate is affected by the different strain partitioning in each phase.

(3) Zener-Hollomon parameter is the primary factor controlling the microstructural evolution, strain partitioning and flow behavior of SDSS2507. As the value of ln$Z$ decreases, the microstructure of ferrite is gradually refined and the grain size of ferrite can be described as a function of ln$Z$.

(4) The dominant softening mechanism of SDSS2507 under varying deformation conditions is composed of DRV and CDRX in ferrite and DDRX in austenite, and is mainly affected by the strain partitioning between ferrite and austenite. At a lower ln$Z$, the strain is almost accommodated by the ferrite and CDRX of ferrite is the dominant softening mechanism. As ln$Z$ increases, the strain partitioning is more uniform and DDRX of austenite is activated, which makes the flow stress decline continuously even at the last stage of compression together with CDRX of ferrite.

References:

[1] C. M. Garzon, A. P. Tschiptschin, Mater. Sci. Eng. A 441 (2006) 230-238.

[2] J. M. Cabrera, A. Mateo, L. Lanes, J. M. Prado, M. Anglada, J. Mater. Process. Technol. 143-144 (2003) 321-325.

[3] Z. G. Song, W. J. Zheng, H. Feng, Z. Z. Wu, H. S. Guo, F. Yu, J. Iron Steel Res. Int. 20 (2013) No. 8, 83-86.

[4] J. O. Nilsson, Mater. Sci. Technol. 8 (1992) 685-700.

[5] A. Iza-Mendia, A. Pinol-Juez, J. J. Urcola, I. Gutierrez, Metall. Mater. Trans. A 29 (1998) 2975-2986.

[6] E. Evangelista, H. J. McQueen, M. Niewczas, M. Cabibbo, Can. Met. Quart. 43 (2004) 339-353.

[7] O. Balancin, W. A. M. Hoffmann, J. J. Jonas, Metall. Mater. Trans. A 31 (2000) 1353-1364.

[8] A. Momeni, S. M. Abbasi, A. Shokuhfar, J. Iron Steel Res. Int. 14 (2007) No. 5, 66-70.

[9] L. F. Li, W. Y. Wang, Z. Q. Sun, Acta Metall. Sin. 39 (2003) 419-425.

[10] D. Zhang, Y. Z. Liu, L. Y. Zhou, Q. Han, B. Jiang, Z. Z. Li, J. Iron Steel Res. Int. 21 (2014) No. 11, 1042-1048.

[11] S. L. Zhu, H. Z. Cao, J. S. Ye, W. H. Hu, G. Q. Zheng, J. Iron Steel Res. Int. 22 (2015) No. 3, 264-271.

[12] L. Chen, X. C. Ma, X. Liu, L. M. Wang, Mater. Des. 32 (2011) 1292-1297.

[13] J. W. Zhao, H. Ding, W. J. Zhao, M. L. Huang, D. B. Wei, Z. Y. Jiang, Comp. Mater. Sci. 92 (2014) 47-56.

[14] Y. H. Yang, B. Yan, Mater. Sci. Eng. A 579 (2013) 194-201.

[15] D. N. Zou, K. Wu, Y. Han, W. Zhang, B. Cheng, G. J. Qiao, Mater. Des. 51 (2013) 975-982.

[16] Y. Y. Liu, H. T. Yan, X. H. Wang, M. Yan, Mater. Sci. Eng. A 575 (2013) 41-47.

[17] G. W. Fan, J. Liu, P. D. Han, G. J. Qiao, Mater. Sci. Eng. A 515 (2009) 108-112.

[18] J. Z. Wang, Z. D. Liu, S. C. Chang, B. H. Sheng, J. Iron Steel Res. Int. 18 (2011) No. 10, 54-58, 79.

[19] X. R. Lei, Q. F. Ding, Y. Y. Chen, X. L. Rui, S. R. Li, Q. F. Wang, J. Iron Steel Res. Int. 20 (2013) No. 6, 38-44.

[20] Y. H. Yang, B. Yan, Mater. Sci. Eng. A 579 (2013) 194-201.

[21] M. Martins, L. C. Casteletti, Mater. Charact. 55 (2005) 225-233.

[22] R. Kaibyshev, K. Shipilova, F. Musin, Y. Motohashi, Mater. Sci. Eng. A 396 (2005) 341-351.

[23] B. Eghbali, A. Abdollah-Zadeh, H. Beladi, P. D. Hodgson, Mater. Sci. Eng. A 435-436 (2006) 499-503.

[24] J. C. Tan, M. J. Tan, Mater. Sci. Eng. A 339 (2003) 124-132.

[25] H. Hallberg, B. Svendsen, T. Kayser, M. Ristinmaa, Comp. Mater. Sci. 84 (2014) 327-338.

[26] H. Beladi, P. Cizek, P. D. Hodgson, Metall. Mater. Trans. A 40 (2009) 1175-1189.

[27] L. Priester, Mater. Sci. Eng. A 309-310 (2001) 430-439.

[28] A. Mirzaei, A. Zarei-Hanzaki, N. Haghdadi, A. Marandi, Mater. Sci. Eng. A 589 (2014) 76-82.

[29] R. C. Souza, E. S. Silva, A. M. Jorge Jr., J. M. Cabrera, O. Balancin, Mater. Sci. Eng. A 582 (2013) 96-107.

[30] P. Cizek, B. P. Wynne, Mater. Sci. Eng. A 230 (1997) 88-94.